Chemical Engineering Journal 446 (2022) 137104

Contents lists available at ScienceDirect

Chemical Engineering Journal

journal homepage: www.elsevier.com/locate/cej

Using silver exchange to achieve high uptake and selectivity for propylene/propane separation in zeolite Y

Ying Xiong [a,*,1], Tian Tian [a], Anouk L'Hermitte [a,b], Alba S.J. Méndez [c], David Danaci [a], Ana E. Platero-Prats [d,e,f], Camille Petit [a,*]

[a] Barrer Centre, Department of Chemical Engineering, Imperial College London, London SW7 2AZ, UK
[b] Department of Materials, Imperial College London, London SW7 2AZ, UK
[c] Deutsches Elektronen-Synchrotron (DESY), Notkestraße 85, 22607 Hamburg, Germany
[d] Departamento de Química Inorgánica, Facultad de Ciencias, Universidad Autónoma de Madrid, Campus de Cantoblanco, Madrid 28049, Spain
[e] Condensed Matter Physics Center (IFIMAC), Universidad Autónoma de Madrid, Campus de Cantoblanco, 28049 Madrid, Spain
[f] Instituto de Investigación Avanzada en Ciencias Químicas de la UAM, Universidad Autónoma de Madrid, Campus de Cantoblanco, 28049 Madrid, Spain

ARTICLE INFO

Keywords:
Propylene/propane separation
Silver exchange
Ag-Y
Propylene uptake
Propylene selectivity

ABSTRACT

Adsorptive separation of propylene and propane, an important step of polypropylene production, is more energy-efficient than distillation. However, the challenge lies in the design of an adsorbent which exhibits both high selectivity and uptake. Herein, we hypothesise that enhancing the propylene affinity of the adsorption sites while keeping a suitable pore size can address this challenge. To do so, we performed silver exchange of a commercial zeolite Y, thereby making the adsorbent design easily scalable. We characterised the adsorbent using analytical, spectroscopic and imaging tools, tested its equilibrium and dynamic sorption properties using volumetric and gravimetric techniques and compared its performance to those of state-of-the-art adsorbents as well as other silver-functionalised adsorbents. The silver-exchanged zeolite Y (Ag-Y) exhibited one of the best selectivity vs uptake performances reported so far. Ag-Y also displayed fast adsorption kinetics and reversible propylene sorption, making it a promising new benchmark for propylene/propane separation. Synchrotron-based pair distribution function analyses identified the silver cations' location which confirmed that the silver sites are easily accessible to the adsorbates. This aspect can, in part, explain the propylene/propane separation performance observed. The overall design strategy proposed here to enhance sorption site affinity and maintain pore size could be extended to other adsorbents and support the deployment of adsorption technology for propylene/propane separation.

1. Introduction

Propylene/propane separation, a necessary step in polypropylene production, relies on distillation, which comes with high energy consumption and infrastructure cost [1]. Adsorptive separation can reduce the energy intensity of the separation process by a factor of ten and offset carbon emissions by a similar amount [2]. In this context, researchers have investigated several adsorbents for this separation, such as zeolites [3–5], metal–organic frameworks (MOFs) [6–10], carbons [11,12], polymers [13,14], silicas [15,16]. From this body of work, they have identified that a trade-off exists between uptake and selectivity for propylene/propane separation materials [6,17,18], i.e., adsorbents exhibiting a high selectivity often possess a low capacity, and vice versa. Indeed, adsorbents with high selectivity typically have narrow pore sizes necessary to discriminate propylene and propane, due to their small and similar kinetic diameters. The narrow pore sizes in turn lead to low uptake and often slow kinetics. On the other hand, larger pores can lead to higher uptake at the expense of selectivity. Low selectivity can result in insufficient purity, and low uptake in poor recovery. Either case compromises the deployment of the adsorbent.

Studies have tried to tackle the above issue, focusing on achieving both high propylene selectivity and uptake. Bachman et al. worked with

* Corresponding authors.
E-mail addresses: ying.xiong@uam.es (Y. Xiong), camille.petit@imperial.ac.uk (C. Petit).
[1] Corresponding author currently at: Departamento de Química Inorgánica, Facultad de Ciencias, Universidad Autónoma de Madrid, Campus de Cantoblanco, Madrid 28049, Spain.

https://doi.org/10.1016/j.cej.2022.137104
Received 7 February 2022; Received in revised form 16 May 2022; Accepted 18 May 2022
Available online 21 May 2022

a MOF series, M_2(m-dobdc) (M = Mn, Fe, Co, Ni; $dobdc^{4-}$ = 4,6-dioxido-1,3-benzenedicarboxylate), that possess increased charge density at the unsaturated metal sites compared to their structural isomer, MOF-74 [6]. The resulting enhanced metal − propylene interactions increased the propylene/propane selectivity while maintaining a high propylene capacity. Liang et al. studied another MOF, Co-gallate, with optimal aperture size and pore confinement for propylene molecules [19], endowing it with high propylene selectivity and acceptable capacity. Recently, we reported a series of silver functionalised hypercrosslinked polymer (HCP)/activated carbon (AC) composites [17]. Owing to the high propylene affinity arising from the silver sites and the enhanced capacity from AC and HCP, the adsorbents overcame the trade-off effect between propylene selectivity and capacity at low pressure range.

Inspired by these former studies, we hypothesise that enhancing the propylene affinity of the adsorption sites while keeping a suitable pore size could lead to a high propylene selectivity and uptake. Here, we propose to test this hypothesis while also focusing on a universal adsorbent design strategy with potential for easy scale-up. For this reason, we opted for a commercial zeolite as the 'backbone' of the adsorbent. Zeolites are well-known for their cation-exchange ability. A priori, one could replace low propylene-affinity cations with high affinity ones via cation exchange, without significantly changing the pore size, provided adequate selection of the exchanged and initial cations. Metal cations such as Ag^+ and Cu^+ exhibit high affinity with olefins. Indeed, they both allow sigma and pi interactions with propylene: (i) σ-bond formation between the filled σ-orbital of the carbon electrons and the empty d or p-orbital of the metal, and (ii) back-donation from the filled metal d-orbital to the empty carbon π*-orbital [20]. While both Ag^+ and Cu^+ could in theory be considered for cation exchange, we selected Ag^+ over Cu^+ as Ag^+ exchange usually requires fewer synthesis steps than Cu^+ exchange, making the whole process easier [21]. Specifically, we conducted silver-exchange on a sodium-form zeolite Y (Na-Y). Na-Y is well-known for its flexible cation exchange behaviour [22] and relatively high surface area [23]. We characterised the silver-exchanged zeolite Y (Ag-Y) using analytical, spectroscopic and imaging tools. Ag-Y exhibited increased propylene selectivity compared to Na-Y, as well as fast adsorption kinetics. Compared to other propylene-selective adsorbents, Ag-Y 'bridged' the selectivity and uptake demonstrated by Fe_2(m-dobdc) and Co-gallate, making it a unique adsorbent with this kind of properties. Ag-Y also showed reversible propylene adsorption over 5 testing cycles. Finally, synchrotron-based pair distribution function (PDF) analyses showed that the silver cations mainly exist at Site II in Ag-Y, making them easily accessible to the adsorbates. Such effect could, in part, explain the good propylene/propane separation performance observed. Overall, the findings show that one could use commercial adsorbents and follow a simple cation exchange procedure to produce an adsorbent with high selectivity and uptake for propylene/propane separation.

2. Experimental section

2.1. Chemicals

All chemicals were obtained from commercial sources and directly used without further purification. Silver nitrate (≥99.0%) was purchased from VWR (Honeywell Fluka, CAS# 7761–88-8). Zeolite Y sodium form (Na-Y, powder, 5.1:1 mol ratio SiO_2:Al_2O_3) was purchased from Alfa Aesar (CAS# 1318–02-1). Silver-exchanged zeolite (granular, +20 mesh) was purchased from Sigma-Aldrich (CAS# 130328–18-6). He and N_2 gas cylinders were purchased from BOC (research grade). Propylene and propane gas cylinders were purchased from Air Liquide (N4.0 grade).

2.2. Silver-exchanged zeolite synthesis

1 g of Na-Y (Na^+) was added to 9 mL of a 0.2 M aqueous solution of silver nitrate. The suspension was then stirred in the dark during 24 h at room temperature. The resulting product was washed using a centrifuge (10 mL water, 3000 rpm for 3 min, three times) and dried in an oven at 333 K for 6 h. The yield was 94.8%.

2.3. Material characterisation

2.3.1. Fourier-transform infrared (FTIR) spectra

Fourier-transform infrared (FTIR) spectra were acquired using a PerkinElmer Spectrum 100 spectrometer equipped with an attenuated total reflectance (ATR) accessory. Sixteen spectra were collected per sample to obtain an averaged spectrum over the wavenumber range of 500 – 4000 cm^{-1} with a resolution of 2 cm^{-1}. The samples were analysed as received/as synthesised.

2.3.2. X-ray photoelectron spectroscopy (XPS)

X-ray photoelectron spectroscopy (XPS) was conducted on a Thermo Scientific K-Alpha$^+$ X-ray photoelectron spectrometer equipped with a MXR3 Al Kα monochromated X-ray source (hυ = 1486.6 eV). The samples were previously ground in an agate mortar, dried in a vacuum oven at 313 K for 24 h, and then mounted onto an XPS sample holder using a conductive carbon tape. Thermo Avantage software was used to process the data for Ag 3*d*. The adventitious carbon (C–C) peak set at 284.8 eV was used for binding energy calibration. A 'Smart' background based on the Shirley background and a Powell algorithm were used for peak fitting.

2.3.3. Thermogravimetric analyses (TGA)

Thermogravimetric analyses (TGA) were performed on a Netzsch TG 209 F1 Libra system. About 10 mg of sample was subjected to a heat treatment from room temperature to 1173 K, at a heating rate of 10 K/min, under a 1 atm N_2 flow (20 mL/min).

2.3.4. Inductively coupled plasma – optical emission spectrometry (ICP-OES)

Inductively coupled plasma - optical emission spectrometry (ICP-OES) was employed for elemental composition and was conducted using the Varian Vista MPX ICP-OES system. The samples were sent for analysis to MEDAC LTD. Prior to the analyses, approximately 15 mg of sample was weighed and digested in a 100 mL aqueous solution containing 5 mL nitric acid and 1 mL hydrofluoric acid.

2.3.5. N_2 Sorption analyses at 77 K

N_2 sorption analyses at 77 K were used to derive the textural properties of the samples. The isotherms were measured volumetrically using a Micromeritics 3Flex gas sorption analyser. Prior to the analyses, about 100–150 mg of sample was evacuated at 333 K under vacuum (0.2 mbar) for 24 h. Then, the samples were degassed in-situ down to 0.003 mbar at a heating rate of 1 K/min up to 393 K, with steps at 353 K, 373 K, 393 K during which the temperature was maintained for 1 h. The temperature was then raised up to 623 K at a heating rate of 5 K/min and maintained for 8 h. The surface area was calculated using the Brunauer-Emmett-Teller (BET) method [24]. The total pore volume was determined from the volume of nitrogen adsorbed at a relative pressure (P/P_0) of 0.97. The pore size distribution (PSD) was derived from the N_2 sorption isotherms at 77 K using the DFT model (N_2 - Cylindrical Pores - Oxide Surface in the 3Flex software version 5.02).

2.3.6. Powder X-ray diffraction (PXRD)

Powder X-ray diffraction (PXRD) measurements were conducted in reflection mode on a PANalytical X'Pert Pro diffractometer with an anode voltage of 40 kV and an emission current of 20 mA, using a monochromatic Cu Kα radiation (λ = 1.54178 Å). The XRD detector was a silicon strip detector X'Celerator. Prior to the analyses, the samples were ground and pressed on a silicon sample holder to form a thin layer.

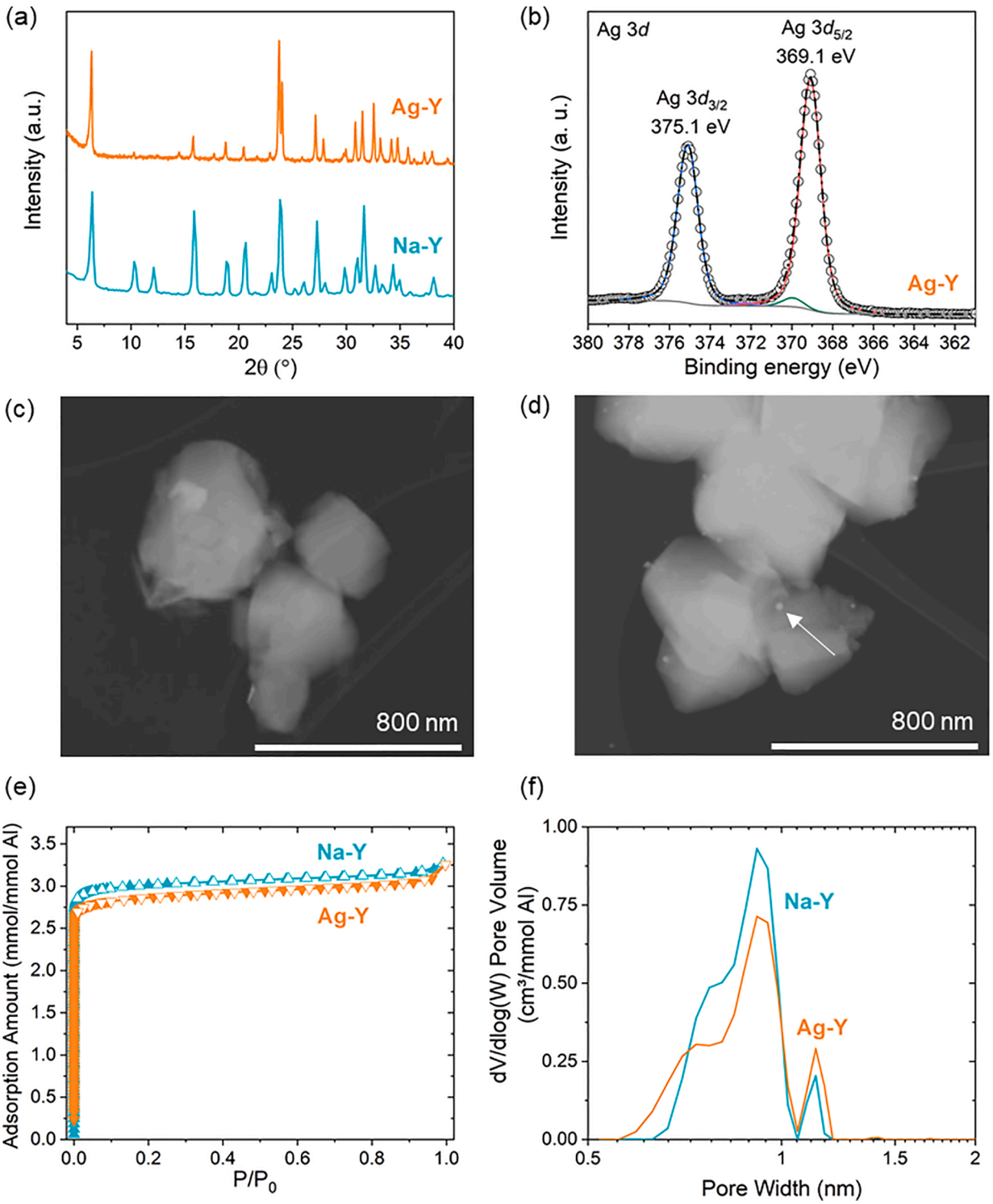

Fig. 1. Characterisation analyses of Ag-Y and Na-Y. (a) PXRD patterns; (b) XPS peaks of Ad 3*d* in Ag-Y; (c) STEM image of Na-Y; (d) STEM image of Ag-Y (arrow points to silver-containing nanoparticle); (e) N_2 sorption isotherms at 77 K with y-axis as mmol/mmol Al (note: the results with y-axis as mmol/g can be found in Fig. S3, the results with x-axis as log scale can be found in Fig. S4); (f) PSD derived from the N_2 sorption isotherms at 77 K using a DFT model (N_2 - Cylindrical Pores - Oxide Surface in the 3Flex software version 5.02).

2.3.7. Scanning transmission electron microscopy (STEM)

Scanning transmission electron microscopy (STEM) analyses were carried out on a JEOL 2100F electron microscope operated at 200 kV. Elemental mapping analyses were performed by Oxford Instruments Aztech. Prior to analysis, the samples were dispersed in water and mounted on carbon tape.

2.4. Equilibrium propylene and propane sorption

The measurements were conducted on a Micromeritics 3Flex gas sorption analyser. The samples were subjected to the same degassing/heating procedure as for the N_2 sorption measurements at 77 K (see Section 2.3.5). The propane and propylene sorption measurements were performed at 288 K, 298 K and 308 K. The data points of the isotherms

can be found in the Supporting Information. The sorption isotherms were used to derive values of selectivity, heat of adsorption and diffusional time constant. The details of the calculations can be found in the Supporting Information (section S1).

2.5. Cyclic propylene adsorption/desorption

The measurement was conducted using a Netzsch TG 209 F1 Libra thermogravimetric analyser. Around 15 mg of Ag-Y was activated by heating in-situ under N_2 flow (20 mL/min) at 5 K/min up to 373 K, with steps at 353 K, 363 K, 373 K during which the temperature was maintained for 1 h. The temperature was then raised up to 623 K at a heating rate of 10 K/min and maintained for 8 h. After that step, the system was allowed to cool down naturally to room temperature. During the adsorption step of the cycle, the sample was first exposed to N_2 at 298 K (15 min, 2 mL/min), then propylene at 298 K (5 h, 2 mL/min). During the desorption step, the sample was exposed to N_2 at 298 K (15 min, 2 mL/min), then heated under N_2 up to 423 K at 1 K/min and up to 623 K at 5 K/min. Finally, the sample was held at 623 K under N_2 for 3 h, before being allowed to cool down naturally to room temperature. These steps represent one adsorption–desorption cycle. The measurement was repeated for five cycles. **Caution note:** the TG outlet must be connected to a ventilation unit and no heating should occur when propylene is flown through the sample chamber. During desorption, N_2 flow and slow heating rate are necessary.

2.6. Pair distribution function analyses

Synchrotron X-ray total scattering data suitable for PDF analyses were measured at the P02.1 beamline at PETRA IIII (Deutsches Elektronen-Synchrotron) using 60 keV (0.20734 Å) X-rays. Samples were loaded in borosilicate capillaries (0.8 mm Ø) and measured by a Varex XRD 4343CT flat panel detector (150 × 150 μm^2 pixel size, 2880 × 2880 pixel area) with a sample-to-detector distance (SDD) of 292 mm and exposure times of 900 s, capturing quarters of the Debye-Scherrer rings. Calibration of the detector and the SDD was performed measuring LaB6 (NIST 660b) as standard material. Geometric corrections and reduction to 1D data were performed by DAWN Science software [25]. PDF results were obtained by PDFgetX3 within xPDFsuite to a $Q_{max} = 25$ $Å^{-1}$ [26]. Differential PDFs were obtained by subtraction of the curve of Na-Y from Ag-Y in real space using Microsoft Excel. The control was multiplied by an appropriate constant to ensure that the scale of each PDF was the same. Simulated PDF results of zeolite Y were obtained by PDFgui [27], the model of zeolite Y containing sodium cations was adopted from [28] and that containing silver cations was adopted from [29].

3. Results and discussion

3.1. Material characterization

We synthesised Ag-Y from Na-Y via cation exchange. Prior to propane and propylene sorption testing, we characterised the Ag-Y and Na-Y samples to assess their chemical and textural properties and confirmed the extent of silver exchange and the nature of the silver species in Ag-Y. The PXRD patterns of Ag-Y displayed similar diffraction peaks to those of Na-Y (Fig. 1a), indicating that Ag-Y maintained the same structure as Na-Y. The reduced intensity of the peaks at 2θ 10.3° and 12.1° in Ag-Y have been reported before [30], and could be related to a partial crystallinity loss or the change of preferred orientation during the silver-exchange process. The N_2 sorption measurements at 77 K further confirmed the integrity of the zeolite upon cation exchange (Fig. 1e and 1f, Fig. S3, Table S1). The Ag-Y sample maintained similar type I isotherm shape and pore size distribution (PSD) to the Na-Y sample. While the absolute porosity of the sample (i.e., per gram of sample) decreased upon cation exchange, the relative porosity (i.e., per mmol of Al site) was preserved. This result demonstrates that no obvious pore blockage was caused by silver exchange. From ICP-OES analyses (Table S2), we also observed a similar Si:Al ratio before and after cation exchange, confirming that the zeolite backbone remained intact. STEM images showed the particle size of Ag-Y is around 0.3 μm (Fig. S6f, g).

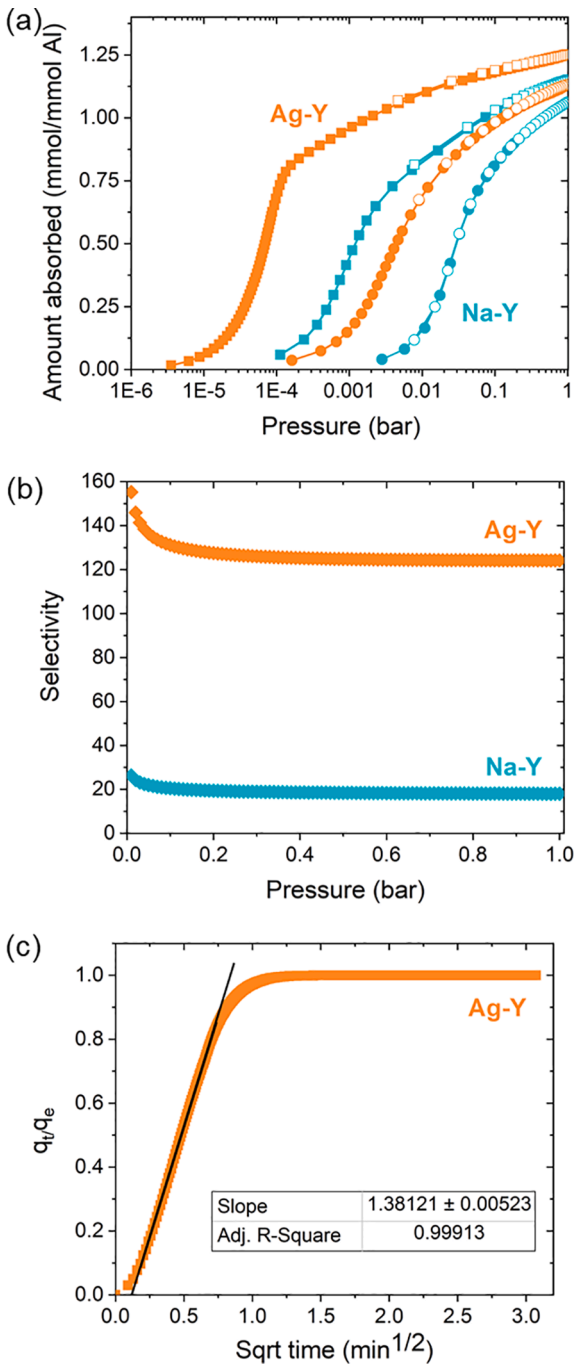

Fig. 2. Equilibrium gas sorption analyses at 298 K. (a) Propylene and propane sorption isotherms of Ag-Y and Na-Y (y-axis as mmol/mmol Al). Square: propylene, circle: propane; solid: adsorption, unfilled: desorption. The results of y-axis as mmol/g and x-axis in linear and log scale are shown in Fig. S10; (b) IAST selectivity of Ag-Y and Na-Y for a propylene:propane ratio of 1:1. The results for a 9:1 ratio are shown in Fig. S14. (c) Adsorption diffusion plot with data points derived from the equilibrium propylene sorption measurement on Ag-Y at 4 × 10^{-6} bar, including linear fitting (black line).

We now focus our attention on the identification and quantification of silver species in Ag-Y. Based on ICP-OES analyses (Table S2), Ag-Y exhibited a Ag:Al ratio of 0.92, indicating that silver almost fully

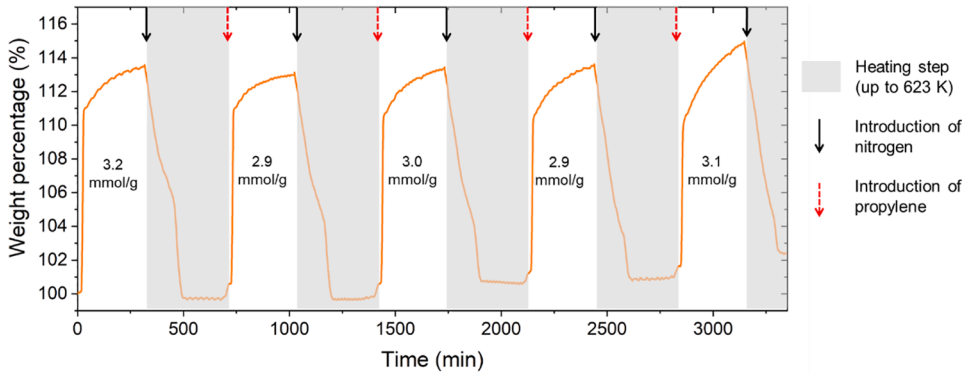

Fig. 3. Propylene adsorption/desorption cycles as measured using a thermogravimetric analyser for Ag-Y. Adsorption steps were conducted at 298 K under a propylene flow. Desorption steps were conducted under a N_2 flow by gradually ramping up the temperature to 623 K.

replaced sodium in zeolite Y. The Ag:Al and Si:Al ratios obtained from XPS analysis (Table S2) were close to those derived from ICP-OES analyses, implying the homogeneity of the sample. To further study the nature of silver in Ag-Y, we used PXRD, XPS and STEM coupled with elemental mapping. We did not identify any peaks from metallic silver or silver oxide from the PXRD patterns (Fig. 1a). The Ag $3d_{5/2}$ and Ag $3d_{3/2}$ XPS peak appeared at 369.1 eV and 375.1 eV, respectively, (Fig. 1b, Fig. S5), and can be assigned to the Ag^+ cations [31,32]. We did not observe peaks related to metallic silver (368.2–368.0 eV) or silver oxide (368.0–367.3 eV) [31]. The STEM images of Ag-Y (Fig. 1d) exhibited a similar particle morphology to that of Na-Y (Fig. 1c), albeit the presence of nanoparticles of ~ 20 nm on the surface of Ag-Y particles. Elemental mapping suggested that these nanoparticles contained mostly silver (Fig. S6a-e). To summarise, the above analyses indicate that silver existed predominantly as Ag^+ replacing original Na^+ of zeolite Y. Yet, a small amount of silver is present as nanoparticles on the surface of Ag-Y, most likely in the form of metallic silver.

Next, we investigated the effect of activation on the nature of the Ag-Y sample prior to adsorption testing. The activation under vacuum and at high temperature (see Experimental section) was necessary owing to zeolite Y's hygroscopic behaviour [33]. For instance, a low activation temperature such as 393 K resulted in only partial activation of the sample, thereby causing a low propane uptake and an overestimation of the propylene/propane selectivity (Fig. S7). After activation at 623 K, Ag-Y turned grey, a phenomenon which could imply the formation of silver nanoparticles [34]. Yet, neither XPS analyses (Fig. S8) nor PXRD patterns (Fig. S9) point to noticeable changes upon activation suggesting that silver still mainly existed as Ag^+ and the Ag-Y framework maintained its integrity upon activation.

3.2. Equilibrium propylene and propane sorption

Having characterised the Ag-Y and Na-Y samples, we then studied their propylene and propane adsorption properties at 298 K. The propylene adsorption isotherm of Ag-Y displayed a steep adsorption step at low pressure until ~ 10^{-4} bar (Fig. 2a, Figs. S10, S12), implying strong interactions between Ag-Y and propylene [35]. This low pressure for the 'initial' adsorption step is the lowest we identified based on current literature. At that pressure, we measured a propylene uptake of 0.9 mol/mol silver, indicating that nearly all silver sites interacted with propylene (the adsorption step finished at 2.1 mmol/g as shown in Fig. S10, silver content calculated based on ICP analyses). Further adsorption beyond 10^{-4} bar may be related to uptake in the empty pore space of Ag-Y. At 1 bar, Ag-Y exhibited a propylene uptake of 1.25 mmol/mmol Al (3.1 mmol/g), as opposed to 1.15 mmol/mmol Al (3.8 mmol/g) for Na-Y.

Beyond uptake, we looked at selectivity, an important metric that influences the purity of the propylene produced. We calculated the IAST

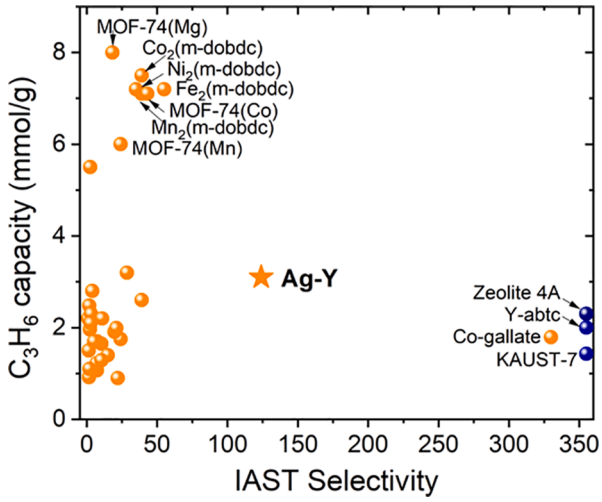

Fig. 4. Propylene uptake vs IAST selectivity (propylene:propane ratio of 1:1) at 1 bar and 298 K for propylene-selective adsorbents. Besides Ag-Y, the named adsorbents are reported in [6,8,19,40]. The unnamed adsorbents are listed in Table S4. Adsorbents that do not adsorb propane, i.e. with undefined IAST selectivity (zeolite 4A [5], KAUST-7 [10], Y-abtc [55]), are shown on the far right in blue colour.

selectivity of Ag-Y and Na-Y for propylene:propane ratios of 1:1 and 9:1 at 298 K. Ag-Y exhibited a selectivity of 124 at 1 bar for a propylene:propane ratio of 1:1. This value was seven times higher that of Na-Y (Fig. 2b). For a propylene:propane ratio of 9:1 at 1 bar, Ag:Y exhibited a selectivity of 124 vs 18 for Na-Y (Fig. S14).

Next, we calculated the heats of adsorption for both Na-Y and Ag-Y for propylene and propane (Figs. S15, S16). While the data tend to suggest a higher heat of adsorption for Ag-Y towards propylene than Na-Y, the points are with the error range (at least partially caused by calculation issues) and do not allow for an unambiguous conclusion at this stage.

3.3. Diffusional time constant

We studied propylene adsorption kinetics in Ag-Y (Fig. 2c, Supporting Information Section S1). The diffusional time constant for propylene reached 2.78 × 10^{-3} s^{-1}. This value compared well with the values reported for other materials in one of our recent studies, which used a similar method to estimate the diffusional time constant [17]. For context, we present the value along with that of other adsorbents in Table S3, showing Ag-Y displays relatively fast adsorption kinetics. However, one must consider that the values reported for these other adsorbents may have been obtained under different conditions and

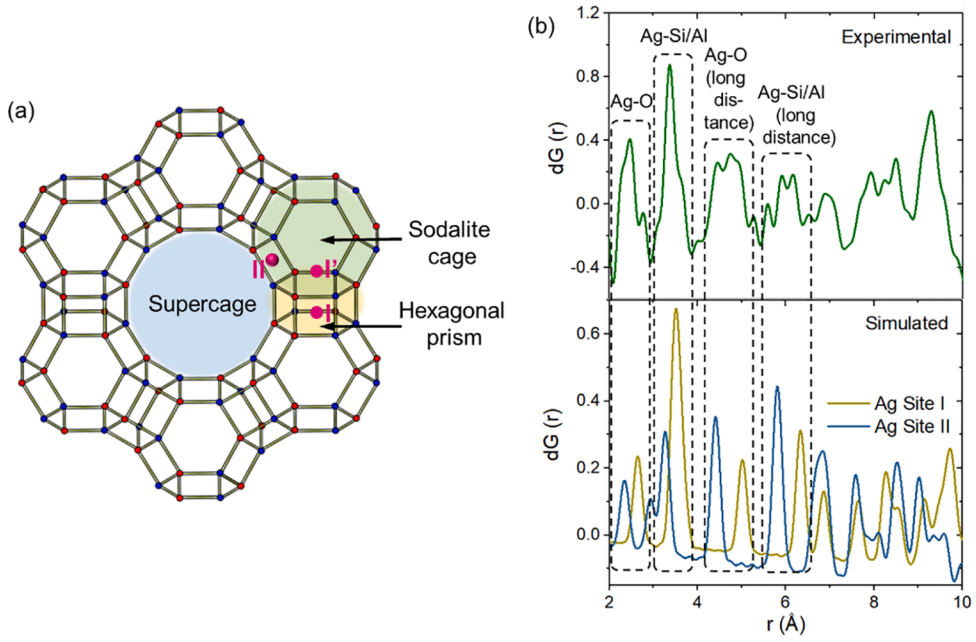

Fig. 5. The positions of silver cations inside Ag-Y by differential-PDF (d-PDF). (a) Structure of zeolite Y showing three possible cation locations (Site I, I' and II) [58]. The subunits of supercage, sodalite cage, and hexagonal prism are marked as blue, green and orange, respectively. (b) Experimental d-PDF signal for the distances of Ag-O and Ag-Si/Al in Ag-Y (up), as well as simulated d-PDF signal for the distances of Ag-O and Ag-Si/Al of silver cations at the Site I and Site II (down).

following a different calculation/estimation method, hence direct comparison may not always be justified.

3.4. Cyclic propylene adsorption/desorption

We performed cyclic propylene adsorption/desorption testing in a dynamic propylene flow to assess Ag-Y recyclability (Fig. 3). Ag-Y displayed a similar propylene uptake to that measured at 1 bar using the gas sorption analyser (3.1 mmol/g). The uptake was maintained over five cycles, showing the reversibility of the propylene adsorption process.

3.5. Comparison with literature

In an attempt to provide perspective on the above results, we compared the propylene uptake and selectivity of Ag-Y with those of other propylene-selective adsorbents whose performance was reported at 298 K and 1 bar [4,6,8,13,14,18,36–53]. We present the results in Fig. 4. Fig. 4 exclude adsorbents exhibiting kinetic separation ability. Overall, we found that Ag-Y exhibited one of the best selectivity vs uptake performances, 'bridging' the MOF-74 and M_2(m-dobdc) series and Co-gallate, and thereby providing a compromise between selectivity and uptake at 298 K, which has not been achieved by other adsorbents before. Considering the superior stability of Ag-Y zeolite compared to MOF-74 series materials [54], Ag-Y may be promising for future industrial application of propylene/propane separation.

The use of silver exchange or doping to produce adsorbents for propylene/propane separation has been reported before [16,56,57]. Yet, the adsorbent investigated here exhibits high propylene uptake and selectivity compared to these adsorbents and a natural question is "Why?". We found that the latter adsorbents might have either exhibited too narrow pores after silver exchange (e.g. Ag_5SiAl_{20} [16], SAM-HCP-Ag-3 [14]) or too large pores (e.g. MC-S-Ag-3 [41], (Cr)-MIL-101-SO_3Ag [56]). Overall, Ag-Y displays the highest propylene selectivity and the third highest capacity among all the silver-containing adsorbents (Tables S5, S6).

We also compared the performance of Ag-Y to that of a commercially available silver-exchanged zeolite. We characterised the latter zeolite using FTIR spectroscopy, TGA, ICP-OES, PXRD and N_2 sorption at 77 K. The results are presented in Figs. S1-S3 and S9 as well as Tables S1-S2. Compared to Ag-Y, the commercial zeolite exhibited a lower porosity and a higher silver content. From a propylene/propane separation perspective, the commercial zeolite performed poorly compared to Ag-Y, despite its higher silver content (Figs. S10, S13, S14). We speculate that its inferior propylene/propane separation ability is due to the low surface area and limited accessibility to the silver sites. We note though that we do not know if the commercial zeolite contained any binder. Overall, our findings point towards the need of suitable pore size and silver content and accessibility to ensure optimal propylene selectivity and uptake.

3.6. The location of silver cations and possible adsorption mechanism

Aiming to gain information on the positions of silver cations inside Ag-Y and further shed light on the mechanism of propylene/propane separation, we applied PDF analyses of X-ray total scattering data on Na-Y (as-synthesised), Ag-Y (as-synthesised), and activated Ag-Y (prepared following the same approach as for gas adsorption tests). The results firstly showed that the average structure of the three samples were overall maintained after silver exchange and thermal activation (Fig. S17). Particularly, no major changes were observed between Ag-Y and activated Ag-Y, once more corroborating that silver predominately exists as cation rather than metallic silver or silver oxide. Secondly, for the structure of Na-Y, the distances of Na-O and Na-Al/Si correspond well with the simulated result obtained from the structure of zeolite Y with Na^+ cations at Site I' and II (Fig. S18), showing that Na^+ cations most likely located at the Site I' and Site II in Na-Y (Fig. 5a).

To study the location of silver sites in Ag-Y, we performed differential-PDFs (d-PDFs) analyses which isolates the environment of silver (the pair of Ag-O and Ag-Si/Al in this study) by subtracting the PDF of Na-Y from that of Ag-Y (Fig. 5b). The d-PDF results showed the peaks of experimental Ag-Y are combinations of the simulated results obtained by Ag^+ cations at Site I and Site II (Fig. 5b), demonstrating that silver cations plausibly exist at Site I and Site II in Ag-Y (Fig. 5a).

To quantitatively analyse the ratio of silver cations at Site I and Site II in Ag-Y, we fitted the peaks related to Ag-Si/Al from 3.1 to 3.9 Å to

Gaussian curves (Fig. S19), the integration areas indicate that the silver cations at Site II account for 75% of the total. We note that Site II can be accessed from the supercage which possesses the largest pore size in zeolite Y. As a result, the majority of Ag^+ cations may be easily accessed and this could contribute to the high propylene capacity and selectivity.

4. Conclusions

In summary, we show that by using a simple silver-exchange procedure and a commercial zeolite Y, we obtain an adsorbent (Ag-Y) for propylene/propane separation that exhibits both high propylene selectivity and capacity compared to its precursor, Na-Y. The combination of a high-affinity adsorption site and suitable pore size confers Ag-Y with one of the best selectivity vs capacity performances reported so far, along with fast adsorption kinetics and reversible propylene adsorption. PDF analyses confirmed that the silver cations are mainly located at positions easily accessible by the adsorbates. Such effect can contribute to the good propylene/propane separation performance observed. The overall adsorbent design strategy demonstrated here could be extended to other adsorbents and the uptake and selectivity obtained could be used for process modelling calculations for further evaluation of the adsorbent performance. Furthermore, one could possibly optimise the adsorbent by studying the partial exchange of Ag-Y, the impact of trace amount of moisture on the separation, as well as extending the design strategy to other cation-exchangeable adsorbents.

Declaration of Competing Interest

The authors declare that they have no known competing financial interests or personal relationships that could have appeared to influence the work reported in this paper.

Acknowledgements

The authors would like to thank Drs L. W. Bolton and Dave Law for their technical input, as well as Dr Mahmoud Ardakani for his assistance in STEM analyses. The authors also acknowledge DESY (Hamburg, Germany), a member of the Helmholtz Association HGF, for the provision of experimental facilities. Parts of this research were carried out at PETRA III beamline P02.1. The authors would also like to acknowledge the funding from bp through the bp International Centre for Advanced Materials (bp-ICAM) (YX, TT, ALH), the Engineering and Physical Sciences Research Council (EPSRC) through the CDT in Advanced Characterisation of Materials (2018 NPIF grant EP/S515085/1) (ALH), the UK Carbon Capture and Storage Research Centre (UKCCSRC, EP/P026214/1) (DD), the Department of Chemical Engineering at Imperial College London (YX), EUR2020-112294 funded by MCIN/AEI/10.13039/501100011033 and by the European Union "NextGenerationEU"/PRTR (A.E.P.-P.), the Spanish Ministry of Science and Innovation through the "María de Maeztu" Programme for Units of Excellence in R&D (CEX2018-000805-M) (A.E.P.-P.), the Spanish Ministry of Science and Innovation for a Ramón y Cajal fellowship (RYC2018-024328-I) (A.E.P.-P.).

Appendix A. Supplementary data

The supplementary material files include: methodology details, materials characterisation analyses (including PDF analyses), additional equilibrium propylene and propene sorption analyses, details of comparison with literature, tabulated sorption data. Supplementary data to this article can be found online at https://doi.org/10.1016/j.cej.2022.137104.

References

[1] B. Liao, Z. Lei, Z. Xu, R. Zhou, Z. Duan, New process for separating propylene and propane by extractive distillation with aqueous acetonitrile, Chem. Eng. J. 84 (3) (2001) 581–586, https://doi.org/10.1016/S1385-8947(01)00175-9.
[2] W.J. Koros, R.P. Lively, Water and beyond: Expanding the spectrum of large-scale energy efficient separation processes, AIChE J. 58 (9) (2012) 2624–2633, https://doi.org/10.1002/aic.13888.
[3] E. Koudelková, Y. Ghrib, F.S. de Oliveira Ramos, P. Čičmanec, R. Bulánek, Adsorption and separation of the C3 hydrocarbons on cationic FER zeolites: Effect of dual sites existence, Microporous Mesoporous Mater. 279 (2019) 416–422, https://doi.org/10.1016/j.micromeso.2019.01.032.
[4] Y. Wu, S. Zeng, D. Yuan, J. Xing, H. Liu, S. Xu, Y. Wei, Y. Xu, Z. Liu, Enhanced Propene/Propane Separation by Directional Decoration of the 12-Membered Rings of Mordenite with ZIF Fragments, Angew. Chem. Int. Ed. 59 (17) (2020) 6765–6768, https://doi.org/10.1002/anie.202000029.
[5] J. Padin, S.U. Rege, R.T. Yang, L.S. Cheng, Molecular sieve sorbents for kinetic separation of propane/propylene, Chem. Eng. Sci. 55 (20) (2000) 4525–4535, https://doi.org/10.1016/S0009-2509(00)00099-3.
[6] J.E. Bachman, M.T. Kapelewski, D.A. Reed, M.I. Gonzalez, J.R. Long, M_2(m-dobdc) (M = Mn, Fe Co, Ni) Metal-Organic Frameworks as Highly Selective, High-Capacity Adsorbents for Olefin/Paraffin Separations, J. Am. Chem. Soc. 139 (43) (2017) 15363–15370, https://doi.org/10.1021/jacs.7b06397.
[7] S.J. Geier, J.A. Mason, E.D. Bloch, W.L. Queen, M.R. Hudson, C.M. Brown, J. R. Long, Selective adsorption of ethylene over ethane and propylene over propane in the metal–organic frameworks M_2(dobdc) (M = Mg, Mn, Fe Co, Ni, Zn), Chem. Sci. 4 (5) (2013) 2054–2061, https://doi.org/10.1039/c3sc00032j.
[8] Y.-S. Bae, C.Y. Lee, K.C. Kim, O.K. Farha, P. Nickias, J.T. Hupp, S.T. Nguyen, R. Q. Snurr, High Propene/Propane Selectivity in Isostructural Metal-Organic Frameworks with High Densities of Open Metal Sites, Angew. Chem. Int. Ed. 51 (8) (2012) 1857–1860, https://doi.org/10.1002/anie.201107534.
[9] Y. He, R. Krishna, B. Chen, Metal–organic frameworks with potential for energy-efficient adsorptive separation of light hydrocarbons, Energy Environ. Sci. 5 (10) (2012) 9107–9120, https://doi.org/10.1039/c2ee22858k.
[10] A. Cadiau, K. Adil, P.M. Bhatt, Y. Belmabkhout, M. Eddaoudi, A metal-organic framework–based splitter for separating propylene from propane, Science 353 (6295) (2016) 137–140, https://doi.org/10.1126/science.aaf6323.
[11] J. Liu, E.M. Calverley, M.H. McAdon, J.M. Goss, Y. Liu, K.C. Andrews, T. D. Wolford, D.E. Beyer, C.S. Han, D.A. Anaya, R.P. Golombeski, C.F. Broomall, S. Sprague, H. Clements, K.F. Mabe, New carbon molecular sieves for propylene/propane separation with high working capacity and separation factor, Carbon 123 (2017) 273–282, https://doi.org/10.1016/j.carbon.2017.07.068.
[12] P. Zhang, X. Wen, L. Wang, Y. Zhong, Y. Su, Y. Zhang, J. Wang, J. Yang, Z. Zeng, S. Deng, Algae-derived N-doped porous carbons with ultrahigh specific surface area for highly selective separation of light hydrocarbons, Chem. Eng. J. 381 (2020), 122731, https://doi.org/10.1016/j.cej.2019.122731.
[13] M.H. Weston, Y.J. Colón, Y.-S. Bae, S.J. Garibay, R.Q. Snurr, O.K. Farha, J.T. Hupp, S.T. Nguyen, High propylene/propane adsorption selectivity in a copper (catecholate)-decorated porous organic polymer, J. Mater. Chem. A 2 (2) (2014) 299–302, https://doi.org/10.1039/c3ta12999c.
[14] A. Stephenson, B. Li, L. Chen, R. Clowes, M.E. Briggs, A.I. Cooper, Efficient separation of propane and propene by a hypercrosslinked polymer doped with Ag (i), J. Mater. Chem. A 7 (44) (2019) 25521–25525, https://doi.org/10.1039/c9ta07510k.
[15] C.A. Grande, J.D.P. Araujo, S. Cavenati, N. Firpo, E. Basaldella, A.E. Rodrigues, New π-Complexation Adsorbents for Propane−Propylene Separation, Langmuir 20 (13) (2004) 5291–5297, https://doi.org/10.1021/la036400s.
[16] M. Kargol, J. Zajac, D.J. Jones, J. Rozière, T. Steriotis, A. Jiménez-López, E. Rodríguez-Castellón, Copper- and Silver-Containing Monolithic Silica-Supported Preparations for Selective Propene−Propane Adsorption from the Gas Phase, Chem. Mater. 17 (24) (2005) 6117–6127, https://doi.org/10.1021/cm051120e.
[17] Y. Xiong, R.T. Woodward, D. Danaci, A. Evans, T. Tian, H. Azzan, M. Ardakani, C. Petit, Understanding trade-offs in adsorption capacity, selectivity and kinetics for propylene/propane separation using composites of activated carbon and hypercrosslinked polymer, Chem. Eng. J. 426 (2021), 131628, https://doi.org/10.1016/j.cej.2021.131628.
[18] Y.-F. Yuan, Y.-S. Wang, X.-L. Zhang, W.-C. Li, G.-P. Hao, L. Han, A.-H. Lu, Wiggling Mesopores Kinetically Amplify the Adsorptive Separation of Propylene/Propane, 60(35) (2021) 19063-19067. https://doi.org/10.1002/anie.202106523.
[19] B. Liang, X. Zhang, Y. Xie, R.-B. Lin, R. Krishna, H. Cui, Z. Li, Y. Shi, H. Wu, W. Zhou, B. Chen, An Ultramicroporous Metal-Organic Framework for High Sieving Separation of Propylene from Propane, J. Am. Chem. Soc. 142 (41) (2020) 17795–17801, https://doi.org/10.1021/jacs.0c09466.
[20] D.J. Safarik, R.B. Eldridge, Olefin/Paraffin Separations by Reactive Absorption: A Review, Ind. Eng. Chem. Res. 37 (7) (1998) 2571–2581, https://doi.org/10.1021/ie970897h.
[21] J.-X. Qin, Z.-M. Wang, X.-Q. Liu, Y.-X. Li, L.-B. Sun, Low-temperature fabrication of Cu(i) sites in zeolites by using a vapor-induced reduction strategy, J. Mater. Chem. A 3 (23) (2015) 12247–12251, https://doi.org/10.1039/C5TA02569A.
[22] A.J. Hernández-Maldonado, R.T. Yang, Desulfurization of Commercial Liquid Fuels by Selective Adsorption via π-Complexation with Cu(I)−Y Zeolite, Ind. Eng. Chem. Res. 42 (13) (2003) 3103–3110, https://doi.org/10.1021/ie0301132.
[23] Y.R. Son, M.-K. Kim, S.G. Ryu, H.S. Kim, Rapid Capture and Hydrolysis of a Sulfur Mustard Gas in Silver-Ion-Exchanged Zeolite Y, ACS Appl. Mater. Interfaces 10 (47) (2018) 40651–40660, https://doi.org/10.1021/acsami.8b15362.

[24] S. Brunauer, P.H. Emmett, E. Teller, Adsorption of Gases in Multimolecular Layers, J. Am. Chem. Soc. 60 (2) (1938) 309–319, https://doi.org/10.1021/ja01269a023.
[25] M. Basham, J. Filik, M.T. Wharmby, P.C.Y. Chang, B. El Kassaby, M. Gerring, J. Aishima, K. Levik, B.C.A. Pulford, I. Sikharulidze, D. Sneddon, M. Webber, S. S. Dhesi, F. Maccherozzi, O. Svensson, S. Brockhauser, G. Naray, A.W. Ashton, Data Analysis WorkbeNch (DAWN), J. Synchrotron Radiat. 22 (3) (2015) 853–858, https://doi.org/10.1107/S1600577515002283.
[26] P. Juhas, T. Davis, C.L. Farrow, S.J.L. Billinge, PDFgetX3: a rapid and highly automatable program for processing powder diffraction data into total scattering pair distribution functions, J. Appl. Crystallogr. 46 (2) (2013) 560–566, https://doi.org/10.1107/S0021889813005190.
[27] C.L. Farrow, P. Juhas, J.W. Liu, D. Bryndin, E.S. Božin, J. Bloch, T. Proffen, S.J. L. Billinge, PDFfit2 and PDFgui: computer programs for studying nanostructure in crystals, J. Phys.: Condens. Matter 19 (33) (2007), 335219, https://doi.org/10.1088/0953-8984/19/33/335219.
[28] S.M. Seo, G.H. Kim, H.S. Lee, S.-O. Ko, O.S. Lee, Y.H. Kim, S.H. Kim, N.H. Heo, W. T. Lim, Single-crystal Structure of Fully Dehydrated Sodium Zeolite Y (FAU), Na_{71}; $[Si_{121}Al_{71}O_{384}]$-FAU, Anal. Sci.: X-ray Struct. Anal. Online 22 (2006) x209–x210, https://doi.org/10.2116/analscix.22.x209.
[29] L.R. Gellens, W.J. Mortier, J.B. Uytterhoeven, Oxidation and reduction of silver in zeolite Y: a structural study, Zeolites 1 (2) (1981) 85–90, https://doi.org/10.1016/S0144-2449(81)80020-6.
[30] X. Chen, B.-X. Shen, H. Sun, G.-X. Zhan, Z.-Z. Huo, Adsorption and Its Mechanism of CS_2 on Ion-Exchanged Zeolites Y, Ind. Eng. Chem. Res. 56 (22) (2017) 6499–6507, https://doi.org/10.1021/acs.iecr.7b00245.
[31] J.F. Moulder, J. Chastain, Handbook of X-ray Photoelectron Spectroscopy: A Reference Book of Standard Spectra for Identification and Interpretation of XPS Data, Physical Electronics Division, Perkin-Elmer Corporation, 1992.
[32] K. Góra-Marek, K.A. Tarach, Z. Piwowarska, M. Łaniecki, L. Chmielarz, Ag-loaded zeolites Y and USY as catalysts for selective ammonia oxidation, Catal. Sci. Technol. 6 (6) (2016) 1651–1660, https://doi.org/10.1039/C5CY01446H.
[33] B. Azambre, M. Chebbi, Evaluation of Silver Zeolites Sorbents Toward Their Ability to Promote Stable CH_3I Storage as AgI Precipitates, ACS Appl. Mater. Interfaces 9 (30) (2017) 25194–25203, https://doi.org/10.1021/acsami.7b02366.
[34] N.D. Hutson, B.A. Reisner, R.T. Yang, B.H. Toby, Silver Ion-Exchanged Zeolites Y, X, and Low-Silica X: Observations of Thermally Induced Cation/Cluster Migration and the Resulting Effects on the Equilibrium Adsorption of Nitrogen, Chem. Mater. 12 (10) (2000) 3020–3031, https://doi.org/10.1021/cm000294n.
[35] M. Kruk, M. Jaroniec, A. Sayari, Adsorption Study of Surface and Structural Properties of MCM-41 Materials of Different Pore Sizes, J. Phys. Chem. B 101 (4) (1997) 583–589, https://doi.org/10.1021/jp962000k.
[36] Y. Wang, N.-Y. Huang, X.-W. Zhang, H. He, R.-K. Huang, Z.-M. Ye, Y. Li, D.-D. Zhou, P.-Q. Liao, X.-M. Chen, J.-P. Zhang, Selective Aerobic Oxidation of a Metal-Organic Framework Boosts Thermodynamic and Kinetic Propylene/Propane Selectivity, Angew. Chem. Int. Ed. 58 (23) (2019) 7692–7696, https://doi.org/10.1002/anie.201902209.
[37] Z. Chang, R.-B. Lin, Y. Ye, C. Duan, B. Chen, Construction of a thiourea-based metal–organic framework with open Ag^+ sites for the separation of propene/propane mixtures, J. Mater. Chem. A 7 (44) (2019) 25567–25572, https://doi.org/10.1039/c9ta08614e.
[38] X. Wang, R. Krishna, L. Li, B. Wang, T. He, Y.-Z. Zhang, J.-R. Li, J. Li, Guest-dependent pressure induced gate-opening effect enables effective separation of propene and propane in a flexible MOF, Chem. Eng. J. 346 (2018) 489–496, https://doi.org/10.1016/j.cej.2018.03.163.
[39] M.-H. Yu, B. Space, D. Franz, W. Zhou, C. He, L. Li, R. Krishna, Z. Chang, W. Li, T.-L. Hu, X.-H. Bu, Enhanced Gas Uptake in a Microporous Metal-Organic Framework via a Sorbate Induced-Fit Mechanism, J. Am. Chem. Soc. 141 (44) (2019) 17703–17712, https://doi.org/10.1021/jacs.9b07807.
[40] Z. Bao, S. Alnemrat, L. Yu, I. Vasiliev, Q. Ren, X. Lu, S. Deng, Adsorption of Ethane, Ethylene, Propane, and Propylene on a Magnesium-Based Metal-Organic Framework, Langmuir 27 (22) (2011) 13554–13562, https://doi.org/10.1021/la2030473.
[41] D. Saha, B. Toof, R. Krishna, G. Orkoulas, P. Gismondi, R. Thorpe, M.L. Comroe, Separation of ethane-ethylene and propane-propylene by Ag(I) doped and sulfurized microporous carbon, Microporous Mesoporous Mater. 299 (2020) 110099–110106, https://doi.org/10.1016/j.micromeso.2020.110099.
[42] J. Yan, B. Zhang, L. Guo, Z. Wang, Highly Selective Adsorption for Ethylene, Propylene, and Carbon Dioxide in Silver-Ionized Microporous Polyimide, J. Phys. Chem. C 123 (1) (2019) 575–583, https://doi.org/10.1021/acs.jpcc.8b10259.
[43] Y. Chen, H. Wu, D. Lv, N. Yuan, Q. Xia, Z. Li, A pillar-layer metal-organic framework for efficient adsorption separation of propylene over propane, Sep. Purif. Technol. 204 (2018) 75–80, https://doi.org/10.1016/j.seppur.2018.04.046.
[44] H. Wu, Y. Yuan, Y. Chen, F. Xu, D. Lv, Y. Wu, Z. Li, Q. Xia, Efficient adsorptive separation of propene over propane through a pillar-layer cobalt-based metal–organic framework, AIChE J. 66 (4) (2020) e16858.
[45] L. Li, R.-B. Lin, X. Wang, W. Zhou, L. Jia, J. Li, B. Chen, Kinetic separation of propylene over propane in a microporous metal-organic framework, Chem. Eng. J. 354 (2018) 977–982, https://doi.org/10.1016/j.cej.2018.08.108.
[46] S. Divekar, A. Nanoti, S. Dasgupta, Aarti, R. Chauhan, P. Gupta, M.O. Garg, S. P. Singh, I.M. Mishra, Adsorption Equilibria of Propylene and Propane on Zeolites and Prediction of Their Binary Adsorption with the Ideal Adsorbed Solution Theory, J. Chem. Eng. Data 61 (7) (2016) 2629–2637.
[47] L. Li, R. Krishna, Y. Wang, J. Yang, X. Wang, J. Li, Exploiting the gate opening effect in a flexible MOF for selective adsorption of propyne from $C_1/C_2/C_3$ hydrocarbons, J. Mater. Chem. A 4 (3) (2016) 751–755, https://doi.org/10.1039/C5TA09029F.
[48] X.-Y. Tian, H.-L. Zhou, X.-W. Zhang, C. Wang, Z.-H. Qiu, D.-D. Zhou, J.-P. Zhang, Two Isostructural Flexible Porous Coordination Polymers Showing Contrasting Single-Component and Mixture Adsorption Properties for Propylene/Propane, Inorg. Chem. 59 (9) (2020) 6047–6052, https://doi.org/10.1021/acs.inorgchem.0c00022.
[49] C.H. Ko, S.-S. Han, J.-H. Park, S.-H. Cho, J.-N. Kim, Silver Nitrate Impregnated Pellet-Type Adsorbents for Propylene/Propane Separation, Ind. Eng. Chem. Res. 45 (26) (2006) 9129–9135, https://doi.org/10.1021/ie051119p.
[50] M. Kargol, J. Zajac, D.J. Jones, T. Steriotis, J. Rozière, P. Vitse, Porous Silica Materials Derivatized with Cu and Ag Cations for Selective Propene−Propane Adsorption from the Gas Phase: Aluminosilicate Ion-Exchanged Monoliths, Chem. Mater. 16 (20) (2004) 3911–3918, https://doi.org/10.1021/cm040051l.
[51] R.T. Yang, E.S. Kikkinides, New sorbents for olefin/paraffin separations by adsorption via π -complexation, AIChE J. 41 (3) (1995) 509–517, https://doi.org/10.1002/aic.690410309.
[52] Q. Dong, Z. Song, F. Zhou, H. Li, M. Yu, Ultrathin, fine-tuned microporous coating modified 5A zeolite for propane/propylene adsorptive separation, Microporous Mesoporous Mater. 281 (2019) 9–14, https://doi.org/10.1016/j.micromeso.2019.02.038.
[53] J.G. Min, K.C. Kemp, S.B. Hong, Propylene/propane separation on a ferroaluminosilicate levyne zeolite, Microporous Mesoporous Mater. 294 (2020) 109833–109839, https://doi.org/10.1016/j.micromeso.2019.109833.
[54] S. Zuluaga, E.M.A. Fuentes-Fernandez, K. Tan, F. Xu, J. Li, Y.J. Chabal, T. Thonhauser, Understanding and controlling water stability of MOF-74, J. Mater. Chem. A 4 (14) (2016) 5176–5183, https://doi.org/10.1039/C5TA10416E.
[55] H. Wang, X. Dong, V. Colombo, Q. Wang, Y. Liu, W. Liu, X.-L. Wang, X.-Y. Huang, D.M. Proserpio, A. Sironi, Y. Han, J. Li, Tailor-Made Microporous Metal-Organic Frameworks for the Full Separation of Propane from Propylene Through Selective Size Exclusion, Adv. Mater. 30 (49) (2018) 1805088, https://doi.org/10.1002/adma.201805088.
[56] G. Chang, M. Huang, Y. Su, H. Xing, B. Su, Z. Zhang, Q. Yang, Y. Yang, Q. Ren, Z. Bao, B. Chen, Immobilization of Ag(i) into a metal–organic framework with –SO_3H sites for highly selective olefin–paraffin separation at room temperature, Chem. Commun. 51 (14) (2015) 2859–2862, https://doi.org/10.1039/c4cc09679g.
[57] J. Padin, R.T. Yang, New sorbents for olefin/paraffin separations by adsorption via π-complexation: synthesis and effects of substrates, Chem. Eng. Sci. 55 (14) (2000) 2607–2616, https://doi.org/10.1016/S0009-2509(99)00537-0.
[58] H. Klein, C. Kirschhock, H. Fuess, Adsorption and Diffusion of Aromatic Hydrocarbons in Zeolite Y by Molecular Mechanics Calculation and X-ray Powder Diffraction, J. Phys. Chem. 98 (47) (1994) 12345–12360, https://doi.org/10.1021/j100098a033.